Check for updates

LASER & PHOTONICS REVIEWS
www.lpr-journal.org

Subwavelength Grating-Assisted Contra-Directional Couplers in Lithium Niobate on Insulator

Xu Han, Yongheng Jiang, Huifu Xiao, Mingrui Yuan, Thach Giang Nguyen, Andreas Boes, Guanghui Ren, Yong Zhang, Qinfen Hao, Yikai Su, Arnan Mitchell, and Yonghui Tian**

Grating-assisted contra-directional couplers are important optical components in photonic integrated circuits (PICs), which can serve as fundamental building blocks for optical (de)multiplexers, switches, filters, and splitters, among others. Recently, lithium niobate on insulator (LNOI) has emerged as an attractive PIC platform with many important active photonic circuit components demonstrated, including electro-optic modulators and second-harmonic wavelength converters. Nevertheless, the LNOI component toolbox still lacks some passive photonic circuit components to fulfill the requirements of future high-performance PICs. In this contribution, a subwavelength grating-assisted contra-directional coupler (GACDC) is proposed, designed, and experimentally demonstrated in a silicon nitride-loaded LNOI waveguide platform. As an example of its applications, a three-channel wavelength-division (de)multiplexer is fabricated and experimentally demonstrated by cascading several GACDCs, with a narrow wavelength spacing of 3.2 nm (400 GHz). The measured device insertion loss of each channel is about 2.5 dB with low interchannel crosstalk below −20 dB. A fabrication tolerance analysis is also carried out, indicating that the proposed GACDCs are tolerant to waveguide width variations.

1. Introduction

Lithium niobate on insulator (LNOI) is an attractive integrated photonic waveguide platform, as it provides optical waveguides that possess a strong electro- and acousto-optic effect, strong optical nonlinearity, wide optical transparency window and offers a high-density integration.[1,2] In the recent few years, a range of photonic integrated circuit (PIC) components has been demonstrated in the LNOI platform, including lasers,[3–8] electro- and acousto-optic modulators,[9–12] and second-harmonic wavelength converters[13–15] among others. Examples are a dual-polarization LNOI coherent electro-optic transmitter has enabled an experimental demonstration with a record single-wavelength data net rate of 1.96 Tb s^{-1}[16] and a record high second-harmonic wavelength conversion efficiency of 2.03×10^{-5} cm^2 GW^{-1} by using an LNOI heterostructure cavity.[17] Though these demonstrations are impressive, the LNOI component toolbox still lacks some passive photonic circuit components, which are important to fulfill the requirements for future high-performance PICs.

Grating-assisted contra-directional coupler (GACDC) is an important optical component, which has widely been investigated in other PIC platforms, since GACDC structures can be used as fundamental building blocks that enable a range of passive devices including optical (de)multiplexer,[18] filter,[19–21] and splitter.[22] Furthermore, the GACDC-based devices usually exhibit advantages such as a flat-top spectral response, high design flexibility and scalability, and free spectrum range (FSR)-free operation. However, challenges remain when realizing GACDC in the LNOI platform. Specifically, the relatively low refractive index of lithium niobate introduces only a small effective index

X. Han, Y. Jiang, H. Xiao, M. Yuan, Y. Tian
School of Physical Science and Technology
Lanzhou University
Lanzhou, Gansu 730000, China
E-mail: siphoton@lzu.edu.cn

X. Han, T. G. Nguyen, A. Boes, G. Ren, A. Mitchell
Integrated Photonics and Applications Centre (InPAC), School of Engineering
RMIT University
Melbourne, VIC 3001, Australia
E-mail: guanghui.ren@rmit.edu.au

A. Boes
School of Electrical and Mechanical Engineering
The University of Adelaide
Adelaide, SA 5005, Australia

Y. Zhang, Y. Su
The State Key Laboratory of Advanced Optical Communication Systems and Networks, Department of Electronic Engineering
Shanghai Jiao Tong University
Shanghai 200240, China

Q. Hao
Institute of Computing Technology
Chinese Academy of Sciences
Beijing 100190, China

The ORCID identification number(s) for the author(s) of this article can be found under https://doi.org/10.1002/lpor.202300203

DOI: 10.1002/lpor.202300203

 © 2023 Wiley-VCH GmbH

18638899, 2023, 10, Downloaded from https://onlinelibrary.wiley.com/doi/10.1002/lpor.202300203 by Shanghai Jiaotong University, Wiley Online Library on [30/10/2023]. See the Terms and Conditions (https://onlinelibrary.wiley.com/terms-and-conditions) on Wiley Online Library for rules of use; OA articles are governed by the applicable Creative Commons License

difference between optical modes in the normal and grating waveguide, which may cause the contra-coupling wavelengths to be located in the stopband of the grating waveguide, resulting in strong Bragg reflection and large device insertion losses.

In this contribution, we propose, design, and experimentally demonstrate an LNOI GACDC, which is achieved by using a subwavelength grating (SWG) waveguide that is coupled to a multimode waveguide, thereby increasing the mode effective index difference. The waveguides are formed by depositing and etching a silicon nitride thin film on the surface of LNOI chip, enabling easy waveguide fabrication by using standard complementary metal-oxide semiconductor-compatible processes. Nevertheless, the optical modes are still strongly confined in the lithium niobate layer to access the excellent material properties of lithium niobate as the silicon nitride has a slightly lower refractive index compared to that of lithium niobate.[23–26] The waveguide widths are designed carefully for a single band coupling with the central wavelength at around 1550 nm. A Gaussian-profile apodization is then applied to the SWG segments to realize a high sidelobe suppression ratio for further device applications. The coupling gap and length are optimized for a relatively low insertion loss and a narrow 3 dB bandwidth. By cascading several our GACDCs, a three-channel wavelength-division (de)multiplexer is realized with a narrow wavelength spacing of 3.2 nm (400 GHz). The measured device insertion loss for each channel is about 2.5 dB with low interchannel crosstalk below −20 dB. The fabrication tolerance analysis indicates that the proposed device is tolerant to waveguide width variations.

2. Operation Principle and Device Design

2.1. Basic Design

Figure 1a shows the schematic diagram of the proposed GACDC consisting of an SWG waveguide, which is coupled to a multimode waveguide. We design the waveguide structures based on a silicon nitride loading layer on the surface of an X-cut LNOI platform. The thicknesses of the lithium niobate and silicon nitride layers are chosen as 300 nm. The detailed parameters of our platform can be found in our previous works.[23,24] In principle, the forward propagating spatial mode in the normal waveguide will be coupled to a backward propagating Bloch mode in the grating waveguide when the phase matching condition is satisfied[18]

$$n_0 + n_{Bloch} = \frac{\lambda_0}{\Lambda} \tag{1}$$

where n_0 and n_{Bloch} are the effective indices of the forward propagating spatial mode and the backward propagating Bloch mode, respectively, λ_0 is the expected coupling wavelength, and Λ is the grating pitch. Besides, it should be noted that the grating waveguide also introduces a photonic stopband, which means the light transmission in the grating waveguide will be rejected when the Bragg condition is satisfied[27]

$$n_{\mathrm{Bloch}} = \frac{\lambda}{2\Lambda} \tag{2}$$

where λ is the central wavelength of the photonic stopband. It can be concluded from Equations (1) and (2) that the mode effective index difference between the forward propagating spatial mode and the backward propagating Bloch mode, i.e., $n_0 - n_{\mathrm{Bloch}}$, is required to be as large as possible. Otherwise, the expected contra-coupling wavelength can be located in the photonic stopband of the grating waveguide, resulting in strong Bragg reflection and large device insertion losses.

However, due to the relatively low refractive index of lithium niobate and silicon nitride, a conventional grating waveguide has typically only a small difference in mode effective index when compared to a single-mode normal waveguide (refer to Section S1, Supporting Information for details). To overcome this limitation, we propose an SWG waveguide with fully etched and isolated segments (refer to Section S1, Supporting Information for details) to reduce the n_{Bloch} and increase the waveguide width of the normal waveguide to increase the n_0, resulting in a waveguide that supports multiple modes.

First, the duty cycle of the SWG waveguide is fixed as 0.5, enabling a relatively low n_{Bloch} while increasing the device feature size simultaneously. As shown in Figure 1b, the mode effective indices in the SWG as a function of waveguide widths are calculated at a wavelength of 1550 nm, by using a full vector eigenmode solver.[28] The SWG width is selected to be w_s = 1.2 μm (<1.8 μm) to satisfy the single-mode condition (supporting TE_0 only). The corresponding n_{Bloch} is calculated to be about 1.763. The gap between the SWG and multimode waveguide is determined by the expected 3 dB bandwidth which can be expressed as[29]

$$\Delta\lambda \propto \frac{1}{L\left|\frac{d}{d\lambda}\left(\left|\beta_0 + \beta_{\mathrm{Bloch}}\right|\right)\right|} \tag{3}$$

where L is the optimal coupling length, β_0 and β_{Bloch} are the propagation constants of the spatial mode and Bloch mode, respectively. To realize a narrow 3 dB bandwidth, the coupling gap is designed as g = 350 nm for a relatively long coupling length. Then, the SWG waveguide is separated from the multimode normal waveguide by using waveguide bending with a radius of r = 200 μm. The SWG tapers are designed to convert the Bloch mode to normal waveguide mode gradually to reduce the mode conversion loss.

The width of the multimode waveguide needs to be considered carefully since an undesired high-order mode in the normal waveguide could accidentally couple to the Bloch mode in the SWG waveguide at undesired wavelengths (refer to Section S2, Supporting Information for details). To analyze our design, we monitored the output spectra by using the finite-difference time domain method (3D-FDTD),[30] when the multimode waveguide width is designed as w_m = 3 μm ($n_0 \approx 1.885$). According to Equation (1), the grating pitch is designed as Λ = 425 nm for an expected coupling wavelength around 1550 nm, and the coupling length L is designed as 765 μm corresponding to 1800 periods. As shown in Figure 1c, unexpected coupling peaks appear at longer wavelengths, which are induced by the high-order modes in the normal waveguide. These coupling peaks can cause undesired crosstalk of GACDC-based devices. To suppress the undesired coupling, we design the width of the multimode waveguide as w_m = 2.1 μm ($n_0 \approx 1.874$ at 1550 nm) which is a special width of mode hybridization. It has been demonstrated in our previous work that the high-order TE mode will be hybridized with

© 2023 Wiley-VCH GmbH

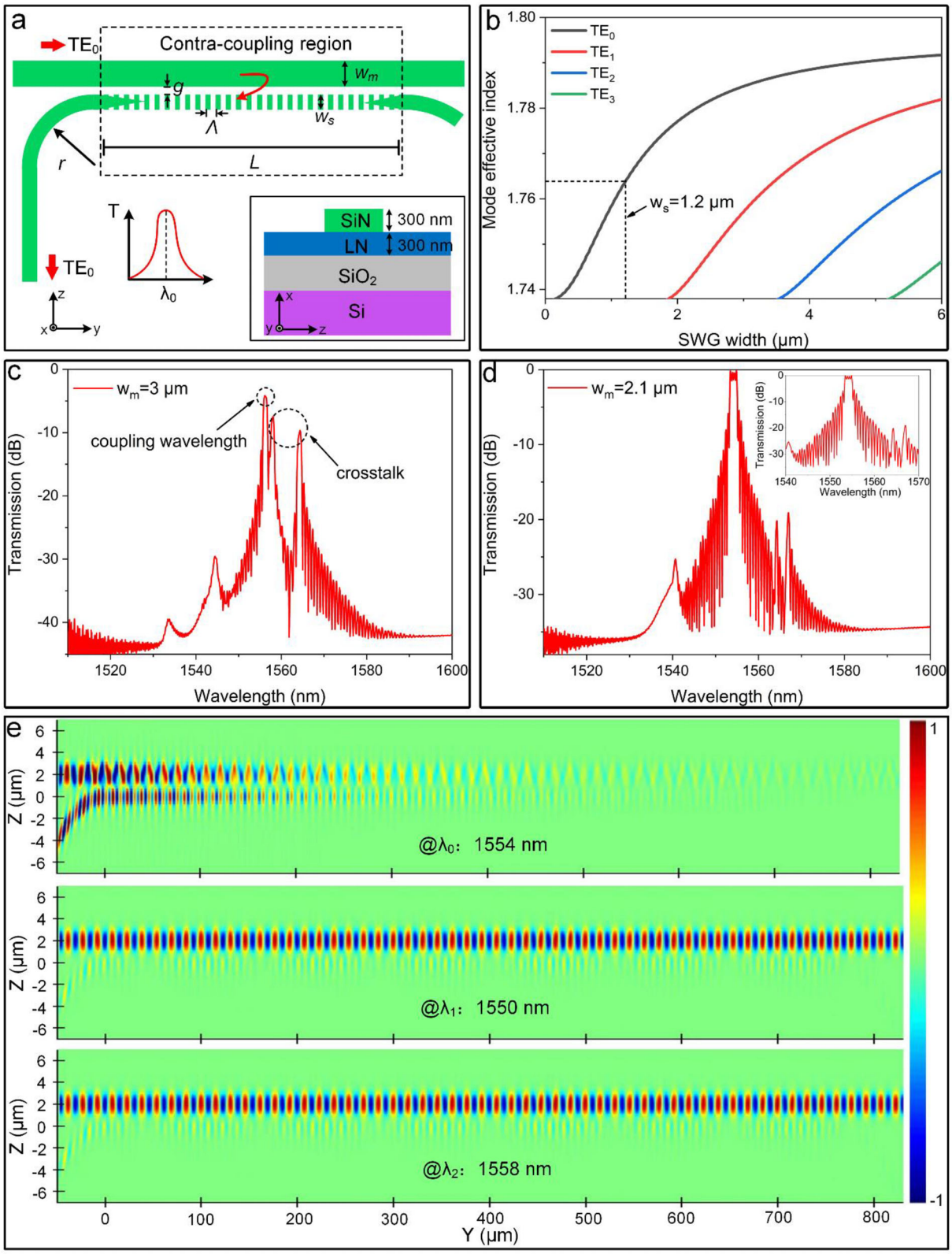

Figure 1. a) The schematic diagram of the proposed GACDC. b) The simulated mode effective index as a function of SWG width, at a wavelength of 1550 nm (the duty cycle of SWG is 0.5). c) The simulated transmission spectrum of the GACDC when the width of normal waveguide is designed as 3 μm. d) The simulated transmission spectra of the GACDC when the width of normal waveguide is designed as 2.1 μm. e) The simulated electric field profiles of the designed GACDC with different wavelengths input.

© 2023 Wiley-VCH GmbH

18638899, 2023, 10, Downloaded from https://onlinelibrary.wiley.com/doi/10.1002/lpor.202300203 by Shanghai Jiaotong University, Wiley Online Library on [30/10/2023]. See the Terms and Conditions (https://onlinelibrary.wiley.com/terms-and-conditions) on Wiley Online Library for rules of use; OA articles are governed by the applicable Creative Commons License

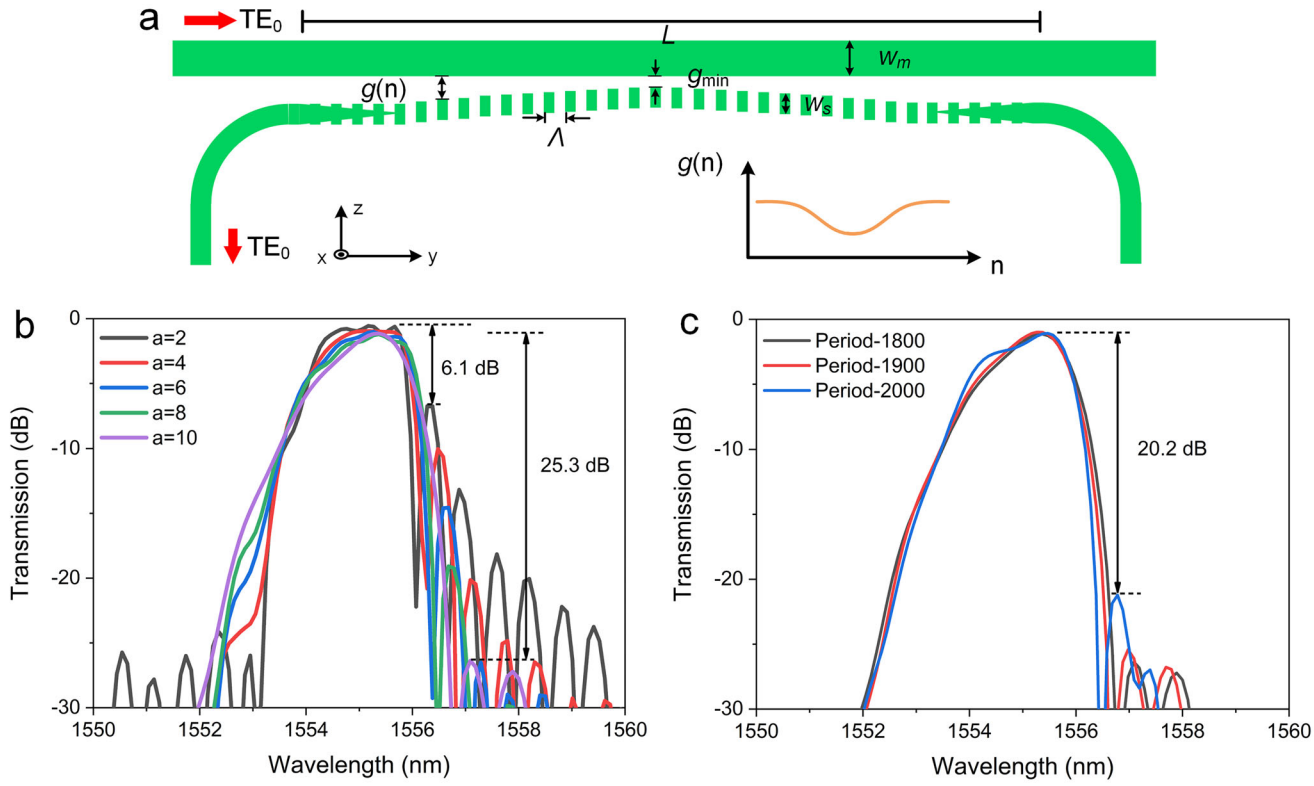

Figure 2. a) The schematic diagram of the proposed GACDC with a Gaussian-profile apodization is designed and applied to the SWG segments. b) The simulated transmission spectra of GACDCs with different apodization indices when the grating number is fixed as 1800. c) The simulated transmission spectra of GACDCs with different grating period number when the apodization index is fixed as 10.

the TM_0 mode at this width, resulting in two hybridized modes with the light polarization undistinguishable.[23] In this case, the mode effective index difference between the hybridized modes in the multimode waveguide and the Bloch mode in the SWG waveguide remains large (refer to Section S2, Supporting Information for details). This results in the undesired coupling being suppressed, due to the phase mismatch,[31] as can be seen in Figure 1d. The designed GACDC shows low-loss and single-band coupling. The simulated insertion loss is about 0.5 dB, and the simulated 3 dB bandwidth is about 1.8 nm. Figure 1e shows the simulated electric field profiles of the designed GACDC structure with different wavelengths input.

2.2. Sidelobe Suppression

Though the GACDC is designed successfully, the simulated transmission spectrum still suffers from the strong sidelobes which can degrade the crosstalk performance. For sidelobe suppression, a Gaussian-profile apodization is designed and applied to the SWG segments for tapering the coupling strength along the waveguides.[20] As shown in **Figure 2**a, the coupling gap between the SWG waveguide and the multimode waveguide as a function of the nth grating period can be given as

$$g(n) = g_{\min} + R\left[1 - e^{\frac{-a(n-0.5N)^2}{N^2}}\right] \quad (4)$$

where $g_{\min}$ is the minimum coupling gap in the center of the contra-coupling region, R is a constant, a is the apodization index, and N is the total grating period number.

In this work, $g_{\min}$ is 350 nm, while R is chosen to be 1. The duty cycle (0.5), grating pitch (Λ = 425 nm), and the widths of the SWG (w_s = 1.2 μm) and normal waveguides (w_m = 2.1 μm) remain the same as that in the basic design. Then we fix the grating period number as 1800 and simulate the transmission spectra of GACDCs with different apodization indices. As shown in Figure 2b, the sidelobe suppression ratio increases from 6.1 to 25.3 dB when the apodization index increases from 2 to 10. However, it can also be seen that a larger apodization index can induce higher insertion loss due to the weaker coupling strength. The simulated insertion loss for a = 2 and a = 10 is about 0.6 and 1.3 dB, respectively. In principle, the insertion loss can be reduced by increasing the coupling length. As shown in Figure 2c, we fix the apodization index as a = 10 and simulate the transmission spectra of GACDCs with different grating period number. According to the results, the insertion loss is slightly reduced while the sidelobes also increase with the coupling length. Thus, there is a trade-off between the high sidelobe suppression and low insertion loss. By considering this trade-off carefully, the finally optimized apodization index is a = 10 and the grating period number is 2000 (L = 850 μm). The simulated minimum insertion loss is about 1 dB, the 3 dB bandwidth is about 1.8 nm, and the sidelobe suppression ratio reaches 20.2 dB.

© 2023 Wiley-VCH GmbH

18638899, 2023, 10, Downloaded from https://onlinelibrary.wiley.com/doi/10.1002/lpor.202300203 by Shanghai Jiaotong University, Wiley Online Library on [30/10/2023]. See the Terms and Conditions (https://onlinelibrary.wiley.com/terms-and-conditions) on Wiley Online Library for rules of use; OA articles are governed by the applicable Creative Commons License

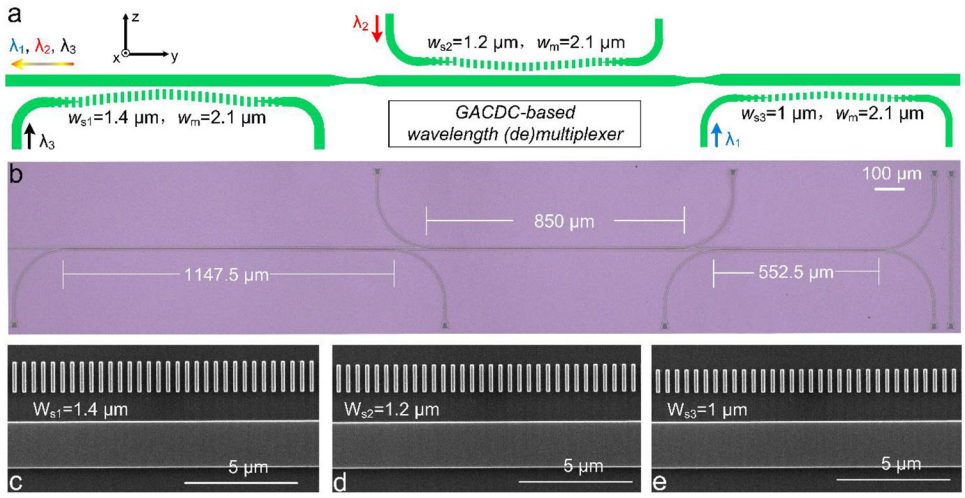

Figure 3. a) The schematic diagram of the proposed GACDC-based wavelength (de)multiplexer. b) The micrograph of the fabricated device. The SEM images of the coupling regions between the multimode normal waveguide and SWG waveguide with a width of c) w_{s1} = 1.4 μm, d) w_{s2} = 1.2 μm, and e) w_{s3} = 1 μm.

3. Fabrication and Device Characterization

As an example of GACDC applications, we use the proposed GACDCs to realize a wavelength-division (de)multiplexer which is one of an important photonic circuit component in optical communication systems. Though the wavelength-division (de)multiplexer has been implemented in LNOI platform by using different structures before,[32–34] the channel spacing remains large (typically 20 nm) in the design for a relaxed requirement of the optical filters. Thus, a narrower channel spacing is still desired to improve the spectrum efficiency and increase the transmission distance limited by the dispersion effect. Though micro-ring resonators are widely investigated as the optical filters when realizing a narrow channel spacing of wavelength-division (de)multiplexer in other platforms,[35–37] a narrow FSR induced by the large bending radius of LNOI waveguide can limit the channel number. Instead, the proposed GACDCs promises to offer an attractive choice of optical filters constructing the wavelength-division (de)multiplexer due to its single-band operation and design flexibility of optical bandwidth.

3.1. Device Fabrication

A GACDC-based wavelength-division (de)multiplexer is designed and fabricated on a silicon nitride-loaded LNOI chip successfully. Three GACDCs working at different wavelengths are cascaded by connecting their multimode normal waveguides after tapering to a single-mode width first, as shown in **Figure 3**a. Figure 3b shows the micrograph of the fabricated device. The LNOI wafer with designed parameters is provided by NanoLN. The silicon nitride thin film is deposited onto the surface of LNOI chip by using the reactive sputtering process.[38] Then, the waveguide structures are pattered and formed by using the electron beam lithography (EBL) followed by the inductively coupled plasma (ICP) etching processes. The measured propagation loss of fabricated waveguide is about 0.25 dB cm^{-1}, by using the cutback method. The device is interfaced by grating couplers which have been developed on the same platform in our previous work.[39] The Y-propagating TE-polarized grating is given a period of 940 nm and a filling factor of 0.4, with a peak coupling efficiency of about −5.94 dB at around 1560 nm.

To realize a wavelength-division (de)multiplexer, the coupling wavelengths of the GACDCs need to be set up with a fixed channel spacing, which can be designed by changing different structural parameters of SWG, including the width, duty cycle, and grating pitch. In this work, the coupling wavelengths are tuned by changing the width of the SWG waveguide, since the slowly varying mode effective index with the width change (see Figure 1b) can provide very fine tuning to achieve a narrow wavelength spacing. According to our simulations, the SWG widths of the GACDCs are designed as w_{s1} = 1.4 μm, w_{s2} = 1.2 μm, and w_{s3} = 1 μm, respectively, with an expected wavelength spacing of about 3.2 nm (400 GHz). Similarly, the apodization index and grating period number of the other two GACDCs are also optimized to obtain high sidelobe suppression ratio and low insertion loss simultaneously. The designed apodization index for w_{s1} = 1.4 μm is a = 14 and the grating period number is 2700 (L = 1147.5 μm), while the designed apodization index for w_{s3} = 1 μm is a = 4 and the grating period number is 1300 (L = 552.5 μm). Figure 3c–e shows the scanning electron microscope (SEM) images of the coupling regions between the multimode normal waveguide and SWG waveguides with different widths.

3.2. Device Characterization and Experimental Results

We characterize the fabricated device by using an amplified spontaneous emission (ASE) source and an optical spectrum analyzer (OSA). In the experiment, the continuous-wave broadband light transmitted from the ASE is coupled into and out of the chip, then received and analyzed by the OSA for transmission spectra characterization.

The simulated and measured normalized transmission spectra are shown in **Figure 4**a,b, respectively. The measured

© 2023 Wiley-VCH GmbH

18638899, 2023, 10, Downloaded from https://onlinelibrary.wiley.com/doi/10.1002/lpor.202300203 by Shanghai Jiaotong University, Wiley Online Library on [30/10/2023]. See the Terms and Conditions (https://onlinelibrary.wiley.com/terms-and-conditions) on Wiley Online Library for rules of use; OA articles are governed by the applicable Creative Commons License

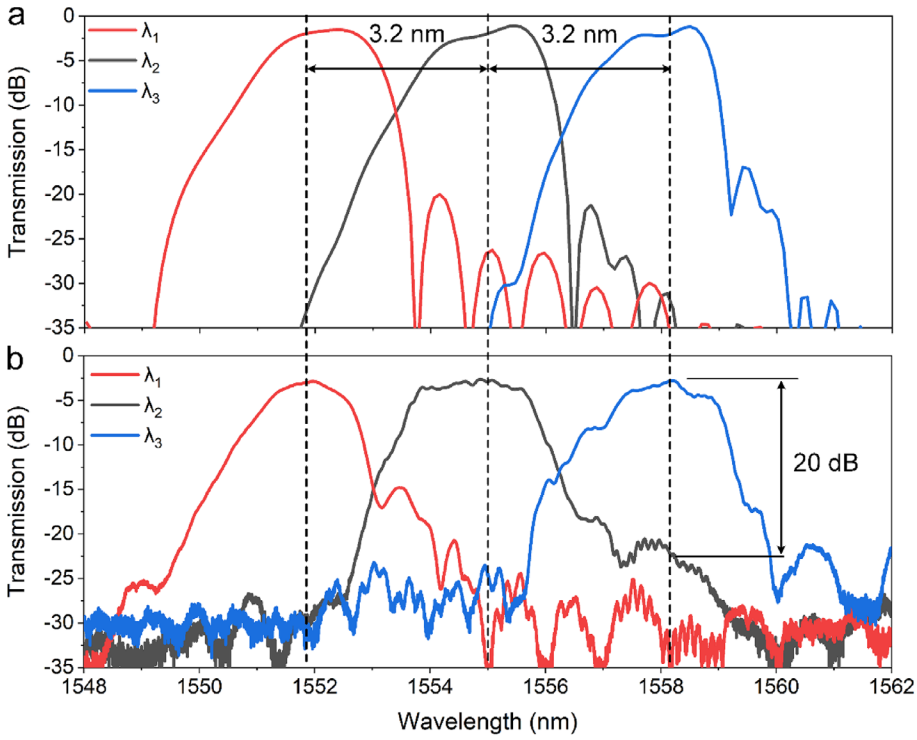

Figure 4. Transmission spectra of the GACDC-based wavelength (de)multiplexer. a) Simulated, b) measured.

Table 1. A summary of the detailed device performance.

Results	Channel spacing	Insertion loss	3 dB bandwidth	Crosstalk
Simulated	3.2 nm	≈1.8 dB	1.8 nm	<−24 dB
Measured	3.2 nm	≈2.5 dB	1.8 nm	<−20 dB

Table 2. A comparison of some reported wavelength-division (de)multiplexers in LNOI.

Reference	Channel spacing	Insertion loss	Crosstalk
[32]	20 nm	<0.72 dB	<−18 dB
[33]	20 nm	<1.08 dB	<−18 dB
[34]	9.6 nm/3.7 nm	<6.6 dB/8.4 dB	<−19.3 dB/−18.3 dB
This work	3.2 nm	≈2.5 dB	<−20 dB

insertion loss of each channel is about 2.5 dB. The measured 3 dB bandwidth is as narrow as about 1.8 nm for each channel, enabling a low interchannel crosstalk below −20 dB. It can be seen that the measured results are overall consistent with the simulated results. For the convenience of comparison, the detailed device performance obtained in the simulation and measurement is included in **Table 1**. The measured larger insertion loss might be caused by the fabrication imperfection in the EBL and ICP processes.

For comparison, we also provide a summary of some previously reported wavelength-division (de)multiplexer in **Table 2**. Though a narrower channel spacing usually requires strict management of the optical filters, it can be seen that this demonstration provides a narrow channel spacing, low insertion loss, and low crosstalk at the telecom band simultaneously when compared with the previously reported works in LNOI.

4. Discussion of Fabrication Tolerance

A potential fabrication deviation can change the coupling wavelength where the phase matching condition (see Equation (1)) is satisfied. In this section, a discussion of fabrication tolerance of the demonstrated GACDC is provided. Though different structural parameters can be considered as the influencing factors, such as the thicknesses of LN and silicon nitride thin films, the etching depth of silicon nitride, and the grating pitch, for simplicity we only considered the effects of waveguide width variations on the coupling wavelengths.

The transmission response of the GACDC to the waveguide width variations is simulated. The simulated transmission spectra are shown in **Figure 5**a for the width variations of $\Delta w = 0$ nm, $\Delta w = \pm 10$ nm, $\Delta w = \pm 20$ nm. It can be seen that the width variations have negligible effects on device performance including insertion loss and 3 dB bandwidth, while the coupling wavelengths are shifted slightly. As shown in Figure 5b, the simulated central wavelength shifts almost linearly with a slope of 0.244 nm/10 nm. Thus, the proposed and demonstrated GACDCs are quite tolerant to the variations in the waveguide width.

5. Conclusion

In summary, we have proposed, designed, and experimentally demonstrated an SWG-based GACDC structure in a silicon

© 2023 Wiley-VCH GmbH

18638899, 2023, 10, Downloaded from https://onlinelibrary.wiley.com/doi/10.1002/lpor.202300203 by Shanghai Jiaotong University, Wiley Online Library on [30/10/2023]. See the Terms and Conditions (https://onlinelibrary.wiley.com/terms-and-conditions) on Wiley Online Library for rules of use; OA articles are governed by the applicable Creative Commons License

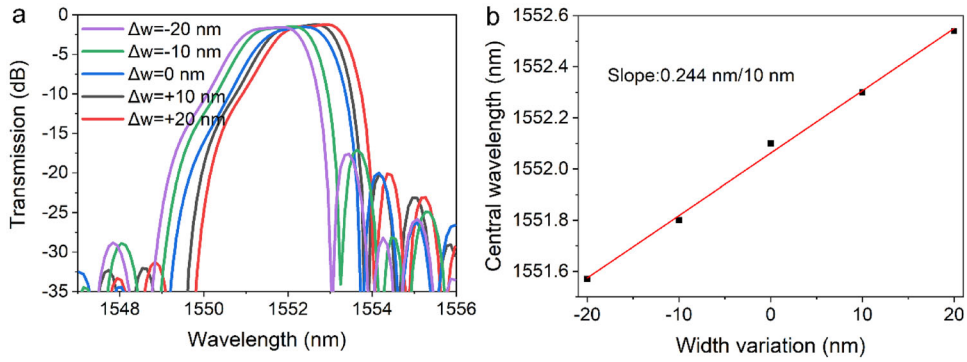

Figure 5. a) Simulated transmission response of the GACDC to the waveguide width variations. b) Simulated and fitted central wavelength shift.

nitride-loaded LNOI platform. The waveguide widths are designed carefully for a single band coupling with the central wavelength at around 1550 nm. A Gaussian-profile apodization has been applied to the SWG segments to realize a high sidelobe suppression ratio. The optimized GACDC shows a minimum insertion loss of about 1 dB and a narrow 3 dB bandwidth of about 1.8 nm. To demonstrate its usefulness, a three-channel wavelength-division (de)multiplexer is realized by cascading several GACDCs, with a narrow wavelength spacing of 3.2 nm (400 GHz). The measured device insertion loss for each channel is about 2.5 dB with low interchannel crosstalk below −20 dB. Furthermore, the proposed GACDC is quite tolerant to variations of the waveguide width. Hence, the demonstrated GACDCs are expected to be a useful photonic circuit component for LNOI platform due to its easy fabrication, high design flexibility, good scalability, and FSR-free operation.

Supporting Information

Supporting Information is available from the Wiley Online Library or from the author.

Acknowledgements

This work was supported by the National Natural Science Foundation of China (NSFC) (62075091), Fundamental Research Funds for the Central Universities (lzujbky-2021-pd11, lzujbky-2022-it32), and Australian Research Council (ARC) grants (DP190102773). The authors acknowledge the facilities and the scientific and technical assistance of the Micro Nano Research Facility (MNRF) and the Australian Microscopy & Microanalysis Research Facility at RMIT University. This work was performed in part at the Melbourne Centre for Nanofabrication (MCN) in the Victorian Node of the Australian National Fabrication Facility (ANFF).

Conflict of Interest

The authors declare no conflict of interest.

Data Availability Statement

The data that support the findings of this study are available from the corresponding author upon reasonable request.

Keywords

contra-directional couplers, lithium niobate on insulator (LNOI), silicon nitride, subwavelength gratings, wavelength-division multiplexing

Received: March 2, 2023
Revised: April 4, 2023
Published online: April 17, 2023

[1] A. Boes, B. Corcoran, L. Chang, J. Bowers, A. Mitchell, *Laser Photonics Rev.* **2018**, *12*, 1700256.
[2] D. Zhu, L. Shao, M. Yu, R. Cheng, B. Desiatov, C. Xin, Y. Hu, J. Holzgrafe, S. Ghosh, A. Shams-Ansari, E. Puma, N. Sinclair, C. Reimer, M. Zhang, M. Lončar, *Adv. Opt. Photonics* **2021**, *13*, 242.
[3] X. Liu, X. Yan, H. Li, Y. Chen, X. Chen, *Opt. Lett.* **2021**, *46*, 5505.
[4] Z. Xiao, K. Wu, M. Cai, T. Li, J. Chen, *Opt. Lett.* **2021**, *46*, 4128.
[5] C. O. de Beeck, F. M. Mayor, S. Cuyvers, S. Poelman, J. F. Herrmann, O. Atalar, T. P. McKenna, B. Haq, W. Jiang, J. D. Witmer, G. Roelkens, A. H. Safavi-Naeini, R. V. Laer, B. Kuyken, *Optica* **2021**, *8*, 1288.
[6] Z. Wang, Z. Fang, Z. Liu, W. Chu, Y. Zhou, J. Zhang, R. Wu, M. Wang, T. Lu, Y. Cheng, *Opt. Lett.* **2021**, *46*, 380.
[7] A. Shams-Ansari, D. Renaud, R. Cheng, L. Shao, L. He, D. Zhu, M. Yu, H. R. Grant, L. Johansson, M. Zhang, M. Lončar, *Optica* **2022**, *9*, 408.
[8] V. Snigirev, A. Riedhauser, G. Lihachev, M. Churaev, J. Riemensberger, R. Wang, A. Siddharth, G. Huang, C. Möhl, Y. Popoff, U. Drechsler, D. Caimi, S. Hönl, J. Liu, P. Seidler, T. J. Kippenberg, *Nature* **2023**, *615*, 411.
[9] C. Wang, M. Zhang, X. Chen, M. Bertrand, A. Shams-Ansari, S. Chandrasekhar, P. Winzer, M. Lončar, *Nature* **2018**, *562*, 101.
[10] A. E. Hassanien, S. Link, Y. Yang, E. Chow, L. L. Goddard, S. Gong, *Photonics Res.* **2021**, *9*, 1182.
[11] M. Xu, M. He, H. Zhang, J. Jian, Y. Pan, X. Liu, L. Chen, X. Meng, H. Chen, Z. Li, X. Xiao, S. Yu, S. Yu, X. Cai, *Nat. Commun.* **2020**, *11*, 3911.
[12] P. Kharel, C. Reimer, K. Luke, L. He, M. Zhang, *Optica* **2021**, *8*, 357.
[13] J. Lu, J. B. Surya, X. Liu, A. W. Bruch, Z. Gong, Y. Xu, H. X. Tang, *Optica* **2019**, *6*, 1455.
[14] S. Yuan, Y. Wu, Z. Dang, C. Zeng, X. Qi, G. Guo, X. Ren, J. Xia, *Phys. Rev. Lett.* **2021**, *127*, 153901.
[15] L. Wang, X. Zhang, F. Chen, *Laser Photonics Rev.* **2021**, *15*, 2100409.
[16] M. Xu, Y. Zhu, F. Pittalà, J. Tang, M. He, W. C. Ng, J. Wang, Z. Ruan, X. Tang, M. Kuschnerov, L. Liu, S. Yu, B. Zheng, X. Cai, *Optica* **2022**, *9*, 61.
[17] S. Yuan, Y. Wu, Z. Dang, C. Zeng, X. Qi, G. Guo, X. Ren, J. Xia, *Phys. Rev. Lett.* **2021**, *127*, 153901.

© 2023 Wiley-VCH GmbH

18638899, 2023, 10, Downloaded from https://onlinelibrary.wiley.com/doi/10.1002/lpor.202300203 by Shanghai Jiaotong University, Wiley Online Library on [30/10/2023]. See the Terms and Conditions (https://onlinelibrary.wiley.com/terms-and-conditions) on Wiley Online Library for rules of use; OA articles are governed by the applicable Creative Commons License

[18] Y. He, Y. Zhang, H. Wang, L. Sun, Y. Su, *Opt. Lett.* **2020**, *45*, 2846.
[19] W. Shi, H. Yun, C. Lin, J. Flueckiger, N. A. Jaeger, L. Chrostowski, *Opt. Lett.* **2013**, *38*, 3068.
[20] B. Liu, Y. Zhang, Y. He, X. Jiang, J. Peng, C. Qiu, Y. Su, *Opt. Express* **2017**, *25*, 11359.
[21] H. Qiu, J. Niu, X. Liang, X. Shen, T. Dai, P. Yu, R. Cheng, *J. Lightwave Technol.* **2021**, *39*, 5896.
[22] Y. Zhang, Y. He, J. Wu, X. Jiang, R. Liu, C. Qiu, X. Jiang, J. Yang, C. Tremblay, Y. Su, *Opt. Express* **2016**, *24*, 6586.
[23] X. Han, Y. Jiang, A. Frigg, H. Xiao, P. Zhang, T. G. Nguyen, A. Boes, J. Yang, G. Ren, Y. Su, A. Mitchell, Y. Tian, *Laser Photonics Rev.* **2022**, *16*, 2100529.
[24] X. Han, L. Chen, Y. Jiang, A. Frigg, H. Xiao, T. G. Nguyen, A. Boes, J. Yang, G. Ren, Y. Su, A. Mitchell, Y. Tian, *Laser Photonics Rev.* **2022**, *16*, 2200130.
[25] A. N. R. Ahmed, S. Shi, A. Mercante, S. Nelan, P. Yao, D. W. Prather, *APL Photonics* **2020**, *5*, 091302.
[26] L. Chang, Y. Li, N. Volet, L. Wang, J. Peters, J. E. Bowers, *Optica* **2016**, *3*, 531.
[27] P. Cheben, R. Halir, J. H. Schmid, H. A. Atwater, D. R. Smith, *Nature* **2018**, *560*, 565.
[28] T. G. Nguyen, R. S. Tummidi, T. L. Koch, A. Mitchell, *IEEE Photonics Technol. Lett.* **2009**, *21*, 486.
[29] D. Marcuse, *J. Lightwave Technol.* **1987**, *5*, 1773.
[30] R. Scarmozzino, A. Gopinath, R. Pregla, S. Helfert, *IEEE J. Sel. Top. Quantum Electron.* **2000**, *6*, 150.
[31] D. Dai, J. Wang, Y. Shi, *Opt. Lett.* **2013**, *38*, 1422.
[32] G. Chen, Z. Ruan, Z. Wang, P. Huang, C. Guo, D. Dai, K. Chen, L. Liu, *Photonics Res.* **2022**, *10*, 8.
[33] Y. Liu, X. Huang, H. Guan, Z. Yu, Q. Wei, Z. Fan, W. Han, Z. Li, *Opt. Lett.* **2021**, *46*, 4726.
[34] Y. Yu, Z. Yu, Z. Zhang, H. K. Tsang, X. Sun, *ACS Photonics* **2022**, *9*, 3253.
[35] R. Boeck, J. Flueckiger, L. Chrostowski, N. A. F. Jaeger, *Opt. Express* **2013**, *21*, 9103.
[36] Y. Tan, H. Wu, S. Wang, C. Li, D. Dai, *Opt. Lett.* **2018**, *43*, 1962.
[37] Y. Tan, H. Wu, D. Dai, *J. Lightwave Technol.* **2018**, *36*, 2051.
[38] A. Frigg, A. Boes, G. Ren, I. Abdo, D.-Y. Choi, S. Gees, A. Mitchell, *Opt. Express* **2019**, *27*, 37795.
[39] X. Han, Y. Jiang, A. Frigg, H. Xiao, P. Zhang, A. Boes, T. G. Nguyen, J. Yang, G. Ren, Y. Su, A. Mitchell, Y. Tian, *APL Photonics* **2021**, *6*, 086108.

© 2023 Wiley-VCH GmbH

18638899, 2023, 10, Downloaded from https://onlinelibrary.wiley.com/doi/10.1002/lpor.202300203 by Shanghai Jiaotong University, Wiley Online Library on [30/10/2023]. See the Terms and Conditions (https://onlinelibrary.wiley.com/terms-and-conditions) on Wiley Online Library for rules of use; OA articles are governed by the applicable Creative Commons License